

Magnetic manipulation of diamagnetic droplet on slippery liquid-infused porous surface

Lin Feng , Xin-Yao He, Ji-Long Zhu, and Wan-Yuan Shi *

Key Laboratory of Low-grade Energy Utilization Technologies and Systems of Ministry of Education, School of Energy and Power Engineering, Chongqing University, Chongqing 400044, China



(Received 20 October 2021; accepted 17 May 2022; published 31 May 2022)

Magnetic control is a feasible way to manipulate droplets in various applications. For actuating nonferromagnetic droplets, embedded magnetic particles or marbles that contact the droplet directly have been widely used; however, such strategies tend to result in departure, substrate contamination, and infection of biological samples. Herein we propose a portable and noncontact method for magnetic manipulation of water droplets on slippery liquid-infused porous surfaces by a single magnet. The migration velocity of the water droplet reaches 1 mm/s, which correlates positively with the droplet volume and negatively with the viscosity of the lubricating oils. The effects of droplet volume, viscosity of lubricating oil, and vertical spacing on the critical migration velocity of water droplet are investigated. Combined with experiments, numerical simulations, and theoretical analysis, the migration mechanism of the droplet is analyzed thoroughly. In addition, this method exhibits great potential for transporting low-surface-tension fluids, bubbles, and magnetic nanofluids. The present findings offer potential benefits for the design and application in droplet microfluidics.

DOI: [10.1103/PhysRevFluids.7.053602](https://doi.org/10.1103/PhysRevFluids.7.053602)

I. INTRODUCTION

Controllable mobility of liquid droplets on solid surfaces is crucial for various applications, including anti-icing [1], fog collection [2], dropwise condensation [3,4], and DNA purification [5]. Various approaches have been developed to drive the motion of droplets, such as temperature [6,7], electricity [8], light [9], and magnetism [10]. Among these approaches, magnetically actuated droplets have garnered significant attention because of their safe, economical, and effective features. Accordingly, magnetic fields, generated either by magnets or electromagnets, are widely used for actuating the magnetic droplets [11,12], or magnetic particle embedded droplets [13–15].

Although the previous literature has demonstrated the feasibility of actuating droplets by magnetic fields, magnetic particles are essential for manipulating the nonferromagnetic liquids. The behaviors of target droplets, i.e., transport, split, or rotation, can be controlled by the size and number of magnetic particles [13]. However, during complex manipulations, the magnetic particles tend to depart from droplets which results in poor magnetic actuation performance and even damages the surface features [16,17]. Recently, direct control of the nonferromagnetic droplets by magnetic fields has attracted wide attention. The repeatable deformation of a diamagnetic droplet was observed, which is shortened along the direction of magnetic field lines on a superhydrophobic surface. The droplet can even be pushed away slightly under a large magnetic field gradient generated by high power coils [18], while the sustained and stable migration of droplet has not yet been implemented. In contrast, the motion of a paramagnetic liquid oxygen droplet in the Leidenfrost state was studied

*Corresponding author: shiwy@cqu.edu.cn

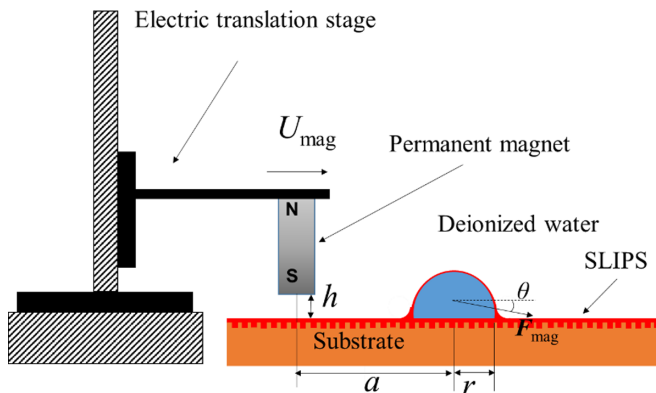


FIG. 1. Schematic of the experimental setup of the migration of water droplet actuated by magnet.

by Piroird *et al.* [19]. Due to its noncontact nature, friction is dramatically reduced and the trajectory of a droplet in the Leidenfrost state was observed to be modified visibly in both the moving direction and velocity by magnetic field generated by a single magnet. Therefore, the substrate heterogeneities, which may result in contact line pinning and impeding the motion of the droplet, has been the critical presupposition for magnetic manipulation of nonferromagnetic droplets.

Surfaces with designed roughness and chemistry, i.e., the superhydrophobic surface, possess remarkable nonwetting properties. The air pockets trapped in the textures enable the surface to exhibit low contact angle hysteresis ($\sim 5^\circ$). However, it is challenging to maintain the stable air-liquid interfaces constantly since the air pockets can be displaced by fluids with low surface tension or damaged by physical interactions [20,21]. An alternative solution was to infuse the air pockets with lubricating fluids which was inspired by the *Nepenthes pitcher* plant, and the slippery liquid-infused porous surface (SLIPS) was proposed [22,23]. On the premise of well-matched solid and liquid surface energies as well as microscale textures, stable liquid-liquid interfaces are formed to achieve further lower contact angle hysteresis ($\sim 2^\circ$) [24]. In the past decade, the single-phase flow and droplet behaviors on SLIPS has been widely investigated [25] and showed promising performance in droplet migration. For instance, the thermocapillary motion of droplet on SLIPS reaches 6.5 mm/s under a temperature gradient of 2 K/mm, which is at least five times quicker than the reported values on conventional surfaces [26]. Although the diamagnetic nature of water and the ultralow friction feature of SLIPS are well known, the effective and continuous droplet actuation by a single magnet on SLIPS remains an open question, and the migration mechanism inside it is unclear. In this study, sustained magnetic manipulation of nonferromagnetic droplets on SLIPS without magnetic particles are realized experimentally. The key factors that affect the motion velocity of the deionized (DI) water droplet are explored and the viscous coefficient is determined. Combined with the numerical simulations and theoretical analysis, we give insight into the mechanism of how the magnet actuates various droplets. In addition, our results demonstrate that the noncontact magnetically actuated droplet on the SLIPS is universal to several types of fluids, such as diamagnetic water droplets, low-surface-tension fluids, magnetic nanofluids, and even bubbles, which offers potential benefits for the design and application in droplet microfluidics.

II. EXPERIMENTAL METHOD

Figure 1 shows the experimental apparatus used in this study. A cylindrical NdFeB (neodymium iron boron) magnet with diameter of 6 mm and height of 19 mm is fixed on an electric translation stage with positional accuracy of $1 \mu\text{m}$ (Shanghai Lianyi Fiber Laser Instrument Co., Ltd.). The chemical etching method is adopted to fabricate micronanoscale grasslike structures on a flat copper surface [4,27]. The organic solvent with 3.3 wt% polytetrafluoroethylene (PTFE) particles with an average diameter of about $10 \mu\text{m}$ is used for hydrophobic coating of the textured surfaces.

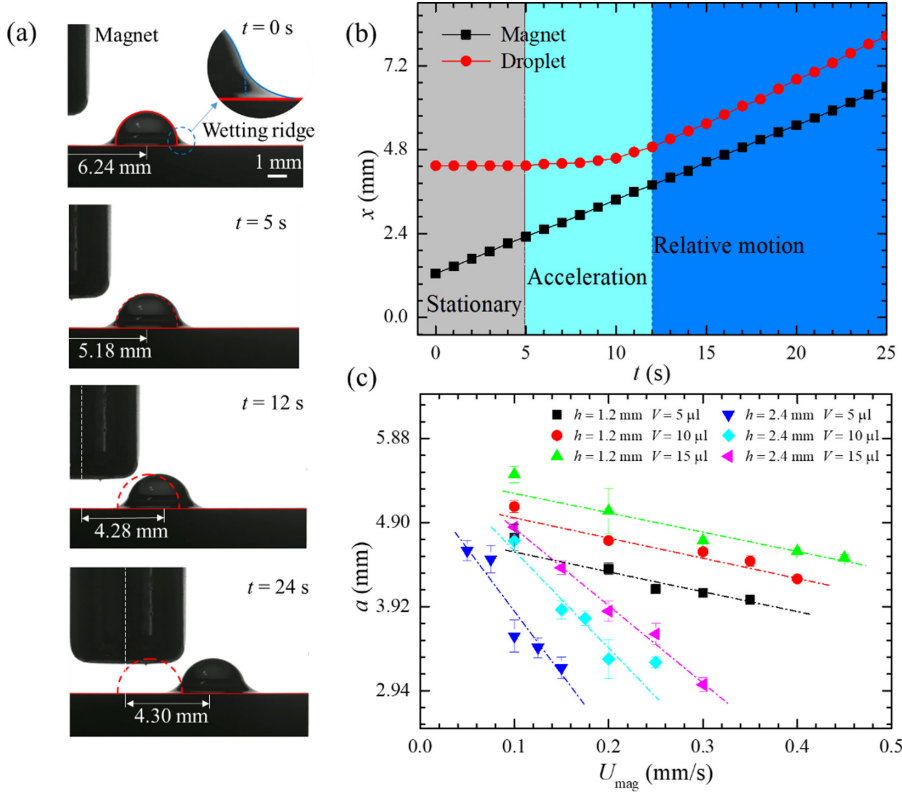


FIG. 2. (a) Migration of 10- μl water droplet driven by the uniform moving magnet under vertical spacing $h = 1.2$ mm. The contact angle of droplet is 100° and the wet radius is 1.56 mm; $t = 0$ –5 s: the droplet remains stationary ($a = 6.24$ mm), $t = 5$ –12 s: the droplet accelerates and the horizontal spacing reduces from 5.18 to 4.28 mm, $t = 12$ –24 s: the droplet remains in relative motion with the magnet, $a = 4.30$ mm, as seen in Supplemental Material Movie S1 [28]. (b) Real-time positions of the magnet and droplet during the motions. (c) Relations of the relative horizontal spacing and moving speed of magnet with respect to droplet volume and vertical spacing.

The sample is then immersed into silicone oil (KF-96L, Shin-Etsu Chemical Co., Ltd.) to form a slippery liquid-infused porous surface (see details in Appendix A). The deionized water droplet with volume of 5–15 μl is predeposited onto the SLIPS using the microsyringe with accuracy of 0.1 μl . The corresponding radius varies from 1.24 to 1.78 mm, which is below the capillary length (~ 2.71 mm) to ensure that the shape of droplet is a spherical cap dominated by surface tension. The water droplet spreads out and stays stationary quickly on the SLIPS. The horizontal spacing a and vertical spacing h between the magnet and water droplet is defined as depicted in Fig. 1. The magnet then moves towards the water droplet with constant velocity of U_{mag} and drives the water droplet forward together. Simultaneously, a contact angle meter (JC2000DM, Shanghai Zhongchen Digital Technic Apparatus Co., Ltd.) with resolution of 0.01° is placed in parallel with the SLIPS to monitor the motion and profile of the droplet.

III. RESULTS AND DISCUSSION

A. Experimental observations

As the magnet moves toward the droplet at a constant speed, three stages are observed during the entire motion of the droplet, as depicted in Figs. 2(a) and 2(b). Initially, the magnet is far away

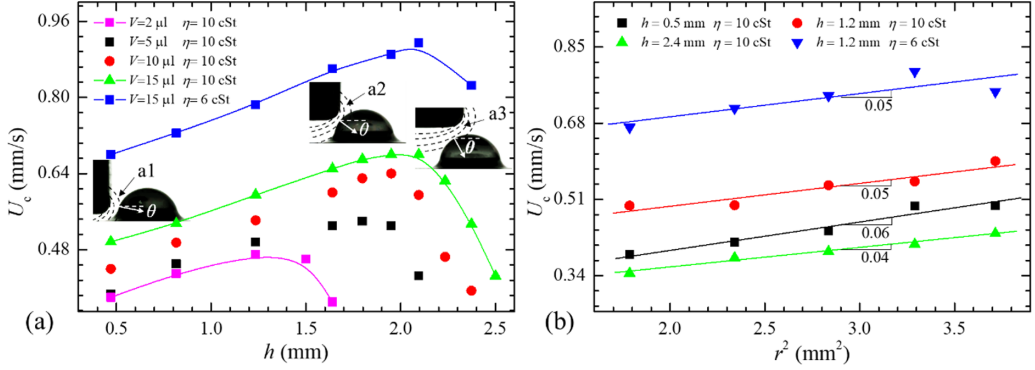


FIG. 3. (a) Critical migration velocity of water droplet as functions of vertical spacing between droplet and SLIPS. The insets donate the cases that the vertical spacing between droplet and magnet is a1: $h = 0.5$ mm; a2: $h = 1.64$ mm and a3: $h = 2.4$ mm. The symbol θ represents the angle between magnetic force and horizontal plane. The dash lines are magnetic flux generated by magnet. (b) Relations of the critical migration velocity of water droplet to the square of droplet radius under various vertical spacings and viscosity of lubricating oil. The slopes of the plotted lines are around 0.05.

from the droplet, and as it approaches gradually, the droplet remains stationary, and the horizontal spacing between the droplet and magnet remains unchanged ($t = 0-5$ s). At the next moment, the droplet is repelled by the magnet owing to the negative nature of the volume magnetic susceptibility $\chi_{\text{water}} = -9.04 \times 10^{-6}$, and the droplet starts out in the same direction as the magnet. During this stage, the droplet accelerates continuously and the horizontal spacing reduces from 5.18 to 4.28 mm ($t = 5-12$ s). Finally, the droplet moves at the same speed as the magnet, and the horizontal spacing remains steady ($t = 12-24$ s). In the following discussion, the horizontal spacing a denotes the steady value, unless stated.

During the motion of the water droplet, the horizontal spacing a between the droplet and magnet shows a significant negative correlation with the moving speed of the magnet, as depicted in Fig. 2(c). This can be attributed to the increased viscous force. As long as the droplet is deposited on the SLIPS, the wetting ridge appears near the triple line of the droplet, as shown in the inset of Fig. 2(a). For a droplet traveling on the SLIPS, the viscous force originates from three parts: the viscous friction in the water droplet, oil film beneath the droplet, and wetting ridge at the contact line. The total viscous resistance can be expressed as $F_{\text{vis}} = \pi\alpha(\rho_o\eta_o + 2\rho_w\eta_w)UR$, where α denotes the experimentally determined prefactor [26]. Thus, with the increase in droplet migration velocity, that is, the moving speed of the magnet, the viscous force increases linearly, leading to reduced horizontal spacing between the droplet and magnet. With the increase in droplet volume, the slope of the curves increases slightly, but they generally remain parallel.

With an increase in the moving speed of the magnet, the horizontal spacing decreases continuously and eventually collides with the droplet. In the present study, we define the maximum velocity of a water droplet that can be achieved as the critical migration velocity U_c . With the increase in vertical spacing between the magnet and SLIPS, the critical migration velocity first increases, and thereafter declines sharply, as shown in Fig. 3(a). The optimal vertical spacing increases as the droplet volume while it is independent of the viscosity of oil. The maximum moving speed observed in the present work is approximately 1 mm/s at 6 cSt silicone oil, which is comparable to that of thermocapillary force-induced droplet motion on lubricant-impregnated surfaces [26]. A larger migration velocity is expected for oils with lower viscosities. Notably, when the vertical spacing is small, the droplet mainly stays at the side of the magnet [see insets a1 and a2 in Fig. 3(a)] and it moves underneath the magnet gradually with the increase in vertical space [inset a3 in Fig. 3(a)]. In the former case, the angle between the magnetic force and horizontal plane is small, which is favorable for the migration of the droplet. Theoretically, the repelling force acting on the water

droplet is perpendicular to the magnetic lines generated by the magnet. With the increase in vertical spacing, the angle increases gradually, and the horizontal component of the magnetic force declines continuously, leading to a steadily deteriorating ability of the actuating water droplet. As the droplet moves from the side to underneath the magnet, both the horizontal angle and magnetic field force increase simultaneously. The combined effect of the two factors discussed is responsible for the initial increase, followed by a declining trend in the critical migration velocity. In addition, the critical migration velocity exhibits a positive linear correlation with the square of the droplet radius, which is valid for droplets under various vertical spacings and viscosities of the lubricating oil, as depicted in Fig. 3(b).

B. Droplet motion mechanism

For further insights into the mechanisms of magnetically actuated nonferromagnetic liquid droplets, a theoretical analysis is performed. The magnetic force exerted on the droplet can be expressed as follows [29,30]:

$$\mathbf{F}_{\text{mag}} = \int \frac{\chi}{2\mu_0} \nabla \mathbf{B}^2 dV. \quad (1)$$

Notably, \mathbf{B} represents the real magnetic flux density inside the materials rather than the externally imposed magnetic field. Even under uniform magnetic fields, the real magnetic field inside the materials is nonuniform, and a magnetic gradient appears, particularly in the boundary regions. Under such circumstances, the droplet tends to deform, which is known as the moss effect [29,31]. In the case of large magnetic gradients, migration is observed [18]. Combined with the capillary force $\mathbf{F}_{\text{cap}} = \gamma(\cos\theta_r - \cos\theta_a)$ and viscous friction of droplet \mathbf{F}_{vis} on the SLIPS, the force balance of the droplet on a horizontal plane is obtained as follows:

$$\int \frac{\chi}{2\mu_0} \nabla \mathbf{B}^2 \cos\theta dV = k\pi r U (2\rho_w \eta_w + \rho_o \eta_o) + \gamma(\cos\theta_r - \cos\theta_a), \quad (2)$$

where θ_r and θ_a denote the receding and advancing angles of the droplet, respectively. Owing to the low friction nature of the SLIPS, the advancing and receding angles are approximately equal, indicating the negligible effect of capillary force on droplet migration. Owing to the difficulty in measuring the real magnetic field inside a droplet experimentally, it is predicted by three-dimensional simulations (see details in Appendix B). In this way, the magnetic force exerted on the water droplet is obtained. Thus, it is feasible to determine the nondimensionalized formula of the migration velocity U^* , as follows:

$$U^* = \frac{1}{k} F_{x,\text{mag}}^* \quad (3)$$

where $U^* = \frac{Ur}{\eta_w}$ and $F_{x,\text{mag}}^* = \frac{\chi}{2\pi\mu_0} \frac{\int \nabla \mathbf{B}^2 \cos\theta dV}{2\rho_w \eta_w^2 + \rho_o \eta_o \eta_w}$, which represents the dimensionless horizontal component of the magnetic force \mathbf{F}_{mag} . The dimensionless velocity versus magnetic force is plotted in Fig. 4(a). However, the data points exhibit three different curves with slopes of $k_1 = 41.5$, $k_2 = 49.6$, and $k_3 = 52.7$, depending on the vertical spacing h . In addition, a positive intercept is observed, indicating the existence of an additional driving force, particularly in the case of lowest k value. As mentioned, when the vertical spacing is small, the droplet is mainly located on the side of the magnet. Under such circumstances, the wetting ridge on the receding side of the droplet is eminently close to the magnet. Considering the similar volumetric magnetic susceptibility of silicone oil ($\chi_{\text{oil}} = -7.5 \times 10^{-6}$ [32]) to that of water, it is suspected that the wetting ridge is also repelled by the nonuniform magnetic field, and thus, moves together with the droplet. The curves in Fig. 4(a) are thereafter corrected by considering the wetting ridge. The shapes of the wetting ridge are obtained from experimental observations (see Appendix B). As shown in Figs. 4(b)–4(d), the dimensionless velocity exhibits a good linear relationship with the magnetic force, as predicted by Eq. (3), thus confirming our suspicion. The slope of the fitted curve is $k = 57.3$, which is larger

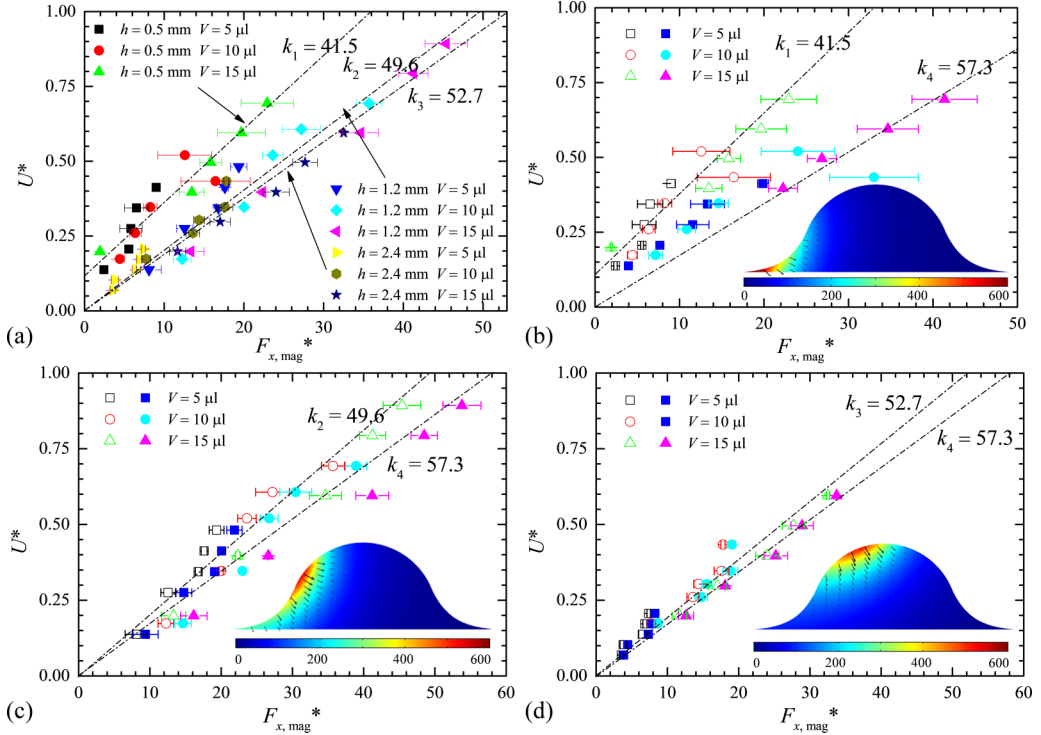


FIG. 4. (a) Dimensionless migration velocity of water droplet as functions of magnetic driving force when the wetting ridge is ignored. (b)–(d) Correction process of the nondimensional magnetic driving force acting on water droplet and wetting ridge under vertical spacing $h = 0.5, 1.2,$ and 2.4 mm. The hollow and solid symbols represent data ignoring and considering the wetting ridge respectively. The symbols are measured in experiments and the dash line represents linear fits using the Levenberg-Marquardt algorithm. The magnetic force distributions are calculated under corresponding vertical spacings and magnet velocity $U_{\text{mag}} = 0.2$ mm/s.

than that of the thermocapillary force-driven water droplet on the SLIPS, $k \approx 22$ [26,27], and a water droplet runs down a declined SLIPS driven by gravity, $k \approx 27$ [24]. As expressed in Eq. (3), the role of k represents the viscous coefficient of the SLIPS under various driving forces, that is, the role of the wetting ridge during the migration of the droplet. In the case of gravity-actuated droplets, the droplet and wetting ridge are relatively independent because they share the same acceleration. Therefore, the wetting ridge does not affect the sliding down of the droplet. For the thermocapillary-force-driven droplet on the SLIPS, the droplet is dragged by the wetting ridge in the advancing direction. Although the wetting ridge functions as a resistance on the receding side of the droplet, the assisting effect on the advancing side dominates. Thus, the total resisting force is weaker than that of the gravity actuated droplet, leading to a smaller k . Similarly, for a magnetically actuated droplet, because the magnetic susceptibility of the water droplet is larger than that of the oil, the magnetic force acting on the droplet is larger than that of the wetting ridge. In our analysis, the ratio of the magnetic driving force inside the wetting ridge to that of the droplet varies from 0.05 to 0.38. Therefore, the wetting ridge is actually dragged by the droplet and the total resisting force becomes larger, resulting in a larger k . Nevertheless, our findings have proved the significance of wetting ridge in transporting droplets on SLIPS. With the assistance of wetting ridge, it is possible to actuate solid samples and bubbles using the method presented in this paper. This provides a potential method of improving the actuation ability by enhancing the magnetic properties of oils.

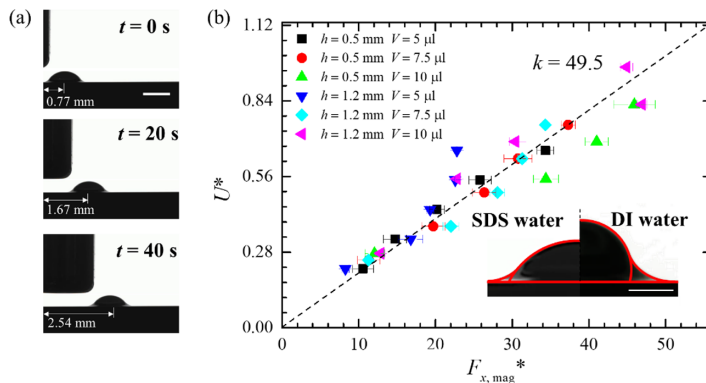


FIG. 5. (a) Migration of a 5- μl SDS water droplet actuated by a magnet moving at a velocity of 0.1 mm/s. The scale bar in the figure is 1 mm (see Supplemental Material Movie S3 [28]). (b) Dimensionless migration velocity of SDS water droplet as functions of magnetic driving force under various vertical spacings and droplet volumes. The symbols are measured in experiments and the dash line represents linear fits using the Levenberg-Marquardt algorithm. The inset donates the experimental observations of the outline of a 5- μl DI water and SDS water droplet and its corresponding wetting ridge.

C. Migration of noncloaked droplet

In the water-oil-air interfaces, the spreading coefficient $S = \gamma_{\text{wa}} - \gamma_{\text{wo}} - \gamma_{\text{oa}} > 0$. Therefore, the water droplet is cloaked by a thin film of silicone oil. Previous studies have confirmed that the cloaking layer has a significant effect on droplet behavior on the SLIPS, such as the inhibition of the evaporation and condensation processes [27,33]. To clarify whether the cloaking layer will affect the magnetic manipulation of the droplet, we add a surfactant (sodium dodecyl sulfate, SDS) to water droplets to lower the interface tension [34]. In this case, the spreading coefficient $S < 0$ and the cloaking layer are removed, which was further confirmed by observing the coalescence behavior of monodisperse microdroplets on the surface of the SDS droplet (see in Appendix C and Supplemental Material Movie S2 [28]). The migration process of SDS water droplets on the SLIPS is investigated under various droplet volumes and vertical spacings, as shown in Figs. 5(a) and 5(b). The linear curve with a slope of $k = 49.5$ is also plotted and exhibits good consistency with the experimental data for SDS water. In comparison with deionized (DI) water, it seems that the SDS water on the SLIPS exhibits lower viscous resistance because the viscous coefficient k is smaller. This can be attributed to the smaller wetting ridge surrounding the SDS droplet due to the weaker spreading coefficient, as depicted in the inset of Fig. 5(b). As discussed, during the migration of the droplet, the interplay between the droplet and wetting ridge leads to an enhanced viscous coefficient. Thus, as the wetting ridge becomes smaller, the slope of the fitted curve declines correspondingly; however, k is still larger than that of water sliding down an inclined surface.

During the entire movement process, no clear deformation of the droplet is observed. This can be partially attributed to the low friction nature of the SLIPS, which prevents the contact line from pinning effectively. In addition, since the size of droplets is smaller than the capillary length, in this circumstance, the shape of the droplet is dominated by surface tension and is less prone to deform. With an increase in the magnetic field, the water droplet tends to be propelled and moves along the magnetic gradient. In our experiments, the maximum magnetic field generated by the magnet is approximately ($\sim 0.4 \text{ T}$, which is much smaller than that reported in the literature ($\sim 1.2 \text{ T}$ [18]). Theoretically, the deformation of a droplet depends on the ratio of the magnetic force to the surface tension, which is determined by the dimensionless magnetic Bond number:

$$B_{0m} = \frac{\chi B_0^2 V^{1/3}}{2\mu_0\gamma}. \quad (4)$$

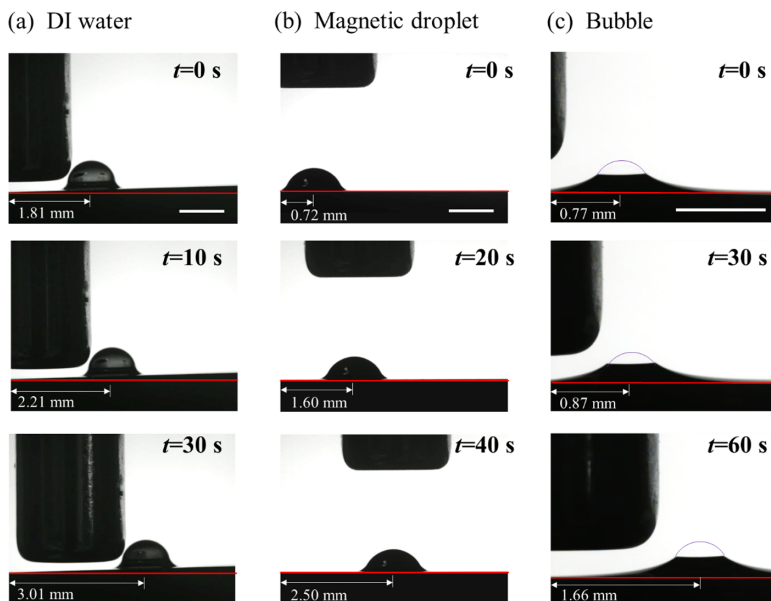


FIG. 6. Migration of (a) water droplet on slightly tilted surface, (b) the magnetic droplet, and (c) bubble actuated by magnet. The sliding angle of SLIPS beneath DI water is 2° . The magnetic droplet used here is the water droplet with Fe_3O_4 10-nm nanoparticles with concentration of 4 mg/ml. The moving velocity of magnet is 0.1 mm/s for DI water and magnet droplet while it is 0.05 mm/s for bubble. The scale bar in figure is 1 mm.

Assigning the properties of water, the maximum value of Bo_m is approximately -0.02 , indicating that the shape of the droplet is still dominated by surface tension. Therefore, the magnetic force cannot deform the shape; however, it can actuate the water droplet easily.

Although magnetic particles offer an efficient strategy for manipulating nonferromagnetic fluids such as water, it is realized by deforming the local outline of the droplet to break the capillary force balance. Consequently, the droplet deforms, splits, or moves as a whole under the action of surface tension. However, such a strategy would be ineffective for manipulating and transporting liquids with ultralow surface tension. In addition, the low surface tension fluids tend to spread out as soon as they are deposited on ordinary solid surfaces, making it hard to form a sessile droplet rather than manipulate it. Notably, the surface tension of the SDS water droplet is approximately $\gamma_{\text{wa}} = 33 \text{ mN/m}$, which is close to that of toluene (28 mN/m) and ethanol (24.8 mN/m). The magnetic manipulation of droplets on the SLIPS provides an effective and efficient solution to this problem. Other droplets, such as the DI water on a slightly tilted surface [Fig. 6(a)], magnetic droplet [Fig. 6(b)], and bubbles [Fig. 6(c)], can also be actuated in a similar way. However, the moving mechanism for three droplets is different. As discussed above, the motion of the DI water droplet mainly relies on the diamagnetic nature of the water droplet. For a magnetic droplet, the magnet generates powerful attractive force and pull the droplet forward. For the air bubbles, the wetting ridge actually plays a key role during the motion. Therefore, the moving velocity is much smaller than that of a DI water droplet. Nevertheless, because most of the organic compounds are diamagnetic, this method is universal for actuating droplets such as proteins, amino acids, and enzymes, thus exhibiting great potential in biology, biomedicine, and pharmaceutical engineering.

IV. CONCLUSIONS

In conclusion, we propose a noncontact magnetically actuated diamagnetic droplet using a moderate magnetic field generated by a single magnet on a SLIPS. Owing to the diamagnetic nature

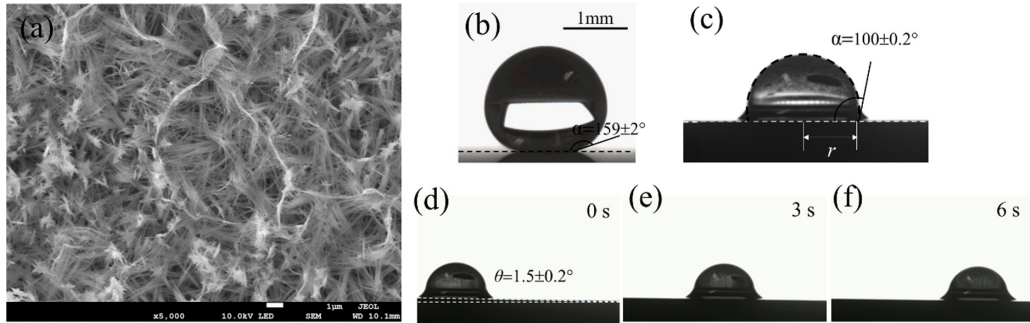


FIG. 7. (a) SEM image of the micronanoscale structures of copper surface. (b) Wetting status of water droplet on PTFE coated surface. (c) Wetting status of water droplet on oil impregnated SLIPS. (d)–(f) Sliding behavior of a water droplet on an inclined SLIPS surface.

of water, a magnetic repulsive force appears as the magnet approaches. The ultralow friction of SLIPS enables a small magnetic force, which is unable to slightly deform the water droplet, to actuate the droplet forward successfully at a velocity of 1 mm/s. With the increase in vertical spacing between the magnet and surface, the droplet moves from the side to the bottom of the magnet, during which the critical migration velocity increases first, followed by a sharp decline. During the motion of droplet, the wetting ridge around the droplet plays a negative role. The viscous coefficient of the DI water droplet and the SDS water droplet actuated by a magnet on a SLIPS are 57.3 and 49.5 respectively, and the difference is attributed to the size of the wetting ridge characterized by spreading coefficient. In addition, this method exhibits great potential for transporting low-surface-tension fluids, bubbles, and magnetic nanofluids, which offer potential benefits for the design and applications of magnetically actuated droplets in droplet microfluidics.

ACKNOWLEDGMENT

This study was funded by the National Natural Science Foundation of China (Grant No. 12002068).

APPENDIX A: SURFACE FABRICATION AND CHARACTERIZATION

The chemical etching method is adopted to fabricate the micronanoscale grasslike structures on flat copper surface. First, a cuboid copper substrate (length \times width \times height = 60 \times 5 \times 20 mm) is sanded with fine-grained sandpaper, then it is immersed into the aqueous solution of hydrochloric acid to dissolve surface oxides. After being cleaned by deionized water, the substrate is then immersed into the aqueous solution of sodium hydroxide (1.25 M) and ammonium peroxodisulfate (0.05 M) for 10 min to generate surface micronanostructures. Next, the substrate is cleaned by deionized water and then dried at 280 °C for 30 min to dehydrate Cu(OH)₂ to CuO. The surface morphology of substrate is characterized by the scanning electron microscope (JEOL JSM-7800F, Japan) at an accelerating voltage of 10 kV, as depicted in Fig. 7(a). To obtain the superhydrophobic wetting feature, the 3.3 wt % PTFE organic solvent is prepared and dipped onto the substrate. After removing the excess solvent by vertical placing for 5 min, the substrate is baked at 280 °C for 30 min to melt the PTFE particles. Followed by nature cooling, superhydrophobic feature of copper surface is achieved and the contact angle of water droplet is about 159° as shown in Fig. 7(b). The slippery liquid-infused porous surface (SLIPS) is thus obtained by immersing the substrate with silicone oil (KF-96L, Shin-Etsu Chemical Co., Ltd.). After the immersion, the sample is vertically oriented on oil-absorbing paper for approximately 10 min to allow gravitational drainage of excess lubricant. Then, there is no apparent oil layer on the surface. The SLIPS is characterized by the wetting ridge

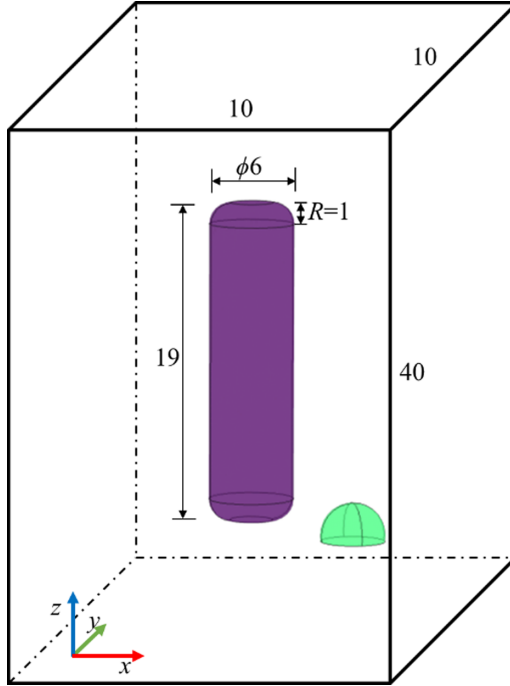


FIG. 8. Schematic diagram of geometric model adopted in simulations. The dimensioned unit is in millimeters.

near the triple line of droplet and the contact angle is about $100 \pm 0.2^\circ$ [in Fig. 7(c)] with a sliding angle of $1.5 \pm 0.2^\circ$ [in Figs. 7(d)–7(f)].

APPENDIX B: NUMERICAL SIMULATIONS

Here we consider a three-dimensional magnetostatics problem whose geometry is shown in Fig. 8. The cylindrical magnet with radius of 1.5 mm and height of 19 mm is positioned in the center of a cuboid box. The upper and lower ends of the magnet are filleted with radius of 1 mm for better consistency with the real magnet in experiments. The magnetization direction of the magnet is assumed to be vertical with magnetization intensity $\mathbf{M}(x, y, z) = (0, 0, 700)$ kA/m. A water droplet with a contact angle of 100° is deposited near the magnet with horizontal spacing a and vertical spacing h . During simulations, the values of a and h are obtained from experiments.

The magnetic field is governed by Maxwell equations for magnetostatics as given by

$$\nabla \cdot \mathbf{B} = 0, \quad (\text{B1})$$

$$\mathbf{B} = \mu \mathbf{H} = \mu_0 (\mathbf{H} + \mathbf{M}), \quad (\text{B2})$$

where \mathbf{B} is the magnetic flux density, \mathbf{H} is the magnetic field intensity, $\mu = \mu_0 \mu_r$ is the magnetic permeability defined by the product of vacuum permeability μ_0 and relative permeability μ_r , $\mathbf{M} = \chi \mathbf{H}$ is the magnetization, and χ is the volumetric magnetic susceptibility. Associated with the magnetic insulating conditions on outer boundaries, the magnetic field generated by a static magnetic is calculated using the finite element method. The total magnetic force that drives the water droplet

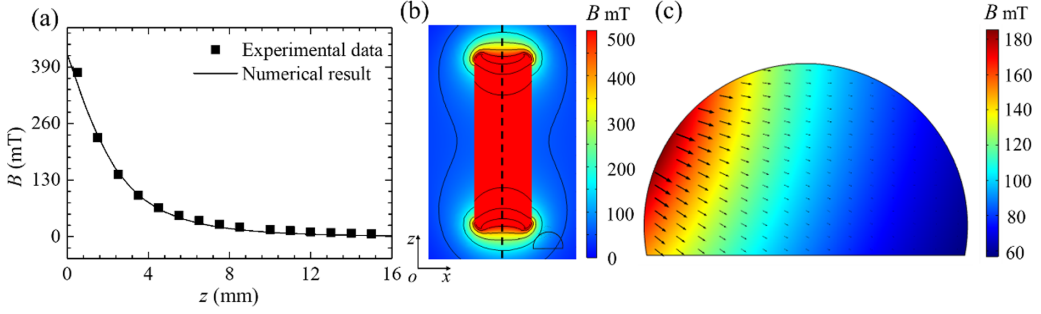


FIG. 9. (a) Comparison of the magnetic flux intensity along the axis of magnet measured by gaussmeter and numerical results. (b) The surrounding magnetic flux distribution of magnet on the z - o - x slice obtained by numerical simulations. (c) The magnetic flux distribution inside water droplet. The arrows indicate the magnetic force induced by magnet.

is given by

$$\mathbf{F}_{\text{mag}} = \int \frac{\chi}{\mu_0} (\mathbf{B} \cdot \nabla) \mathbf{B} dV. \quad (\text{B3})$$

Under the assumption that there is no electric charge over the whole system, we can obtain $\nabla \times \mathbf{B} = 0$. Combining with the identical relation, $\mathbf{B} \times (\nabla \times \mathbf{B}) = 2\nabla(\mathbf{B} \cdot \mathbf{B}) - 2(\mathbf{B} \cdot \nabla)\mathbf{B}$, Eq. (B3) can be further expressed as

$$\mathbf{F}_{\text{mag}} = \int \frac{\chi}{2\mu_0} \nabla B^2 dV. \quad (\text{B4})$$

To confirm the reliability of numerical results, we measured the magnetic flux intensity along the axis of magnet experimentally and compared to the numerical predictions. Good consistency indicates the reliability of the numerical simulations as depicted in Fig. 9(a). Besides, the magnetic flux distribution around the magnet and the magnetic force inside the water droplet are visualized as shown in Figs. 9(b) and 9(c). Under the nonuniform magnetic field generated by the magnet, repelling magnetic force is observed inside the water droplet. It is worth noting that although the moss effect, i.e., the profile of the droplet is deformed by magnetic fields, has been observed in previous works [18], the magnetic force distribution inside the droplet is unknown.

To investigate the influence of the wetting ridge on the migration of water droplet, the outlines of the droplet and the wetting ridge are determined from experiments under different droplet volumes as shown in Fig. 10. Then the shape of wetting ridge is fitted as functions of $f(x) = a\exp(-bx) + c$ [27] and incorporated into numerical simulations to calculate the magnetic force distributions. The corresponding coefficients a , b , and c are determined and listed in Table I.

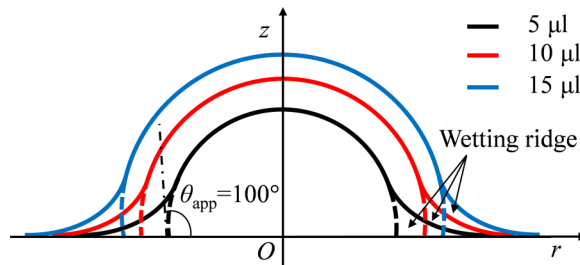


FIG. 10. The outlines of DI water droplet deposited on SLIPS.

TABLE I. Coefficients for exponential fit of wetting ridge under various droplet volume at 95% confidence bounds.

V (μl)	a	b	c	R -square
5	16.63	2.444	-0.0498	0.9945
10	41.81	2.398	-0.0372	0.9970
15	137.4	2.649	-0.03267	0.9973

APPENDIX C: NONCLOAKING BEHAVIOR OF SDS WATER DROPLET ON SLIPS

In the water-oil-air interfaces, $\gamma_{wa} = 72$ mN/m, $\gamma_{wo} = 42$ mN/m, and $\gamma_{oa} = 20.1$ mN/m, the spreading coefficient $S = \gamma_{wa} - \gamma_{wo} - \gamma_{oa} > 0$. Thus, the cloaking effect is expected and a thin oil layer appears on the surface of the droplet. To confirm the influence of the cloaking effect on the magnetic manipulation of the droplet, the sodium dodecyl sulfate (SDS) is added into the water to reduce the interfacial tension of γ_{wa} and γ_{wo} . The concentration is 4.72 g/L, resulting in lowered interfacial tension of $\gamma_{wa} = 33$ mN/m and $\gamma_{wo} = 20$ mN/m. The corresponding spreading coefficient reduces to $S = -7.1$ mN/m. Theoretically, there is no cloaking layer any more. Nevertheless, it is necessary to further confirm the cloaking state of the droplet. Since the cloaking layer is too thin (~ 10 nm), it is hard to detect directly by dyeing. Inspired by the a method in the literature [35], the coalescence behavior of monodisperse microdroplets is observed to help judge the cloaking state of the droplet, as shown in Fig. 11. The microdroplets are produced by a spray gun (S-CP2). For the water droplet, as soon as the microdroplets are sprayed onto the surface, these microdroplets slide down quickly. In contrast, the microdroplets emerge from the droplet and disappear on the surface of SDS water while the microdroplets are observed near the triple line where a wetting ridge exists. This proves that the oil layer exists on the surface of the water droplet and there is no cloaking layer on the surface of the SDS water droplet. Such a conclusion is consistent with the theoretical analysis discussed above.

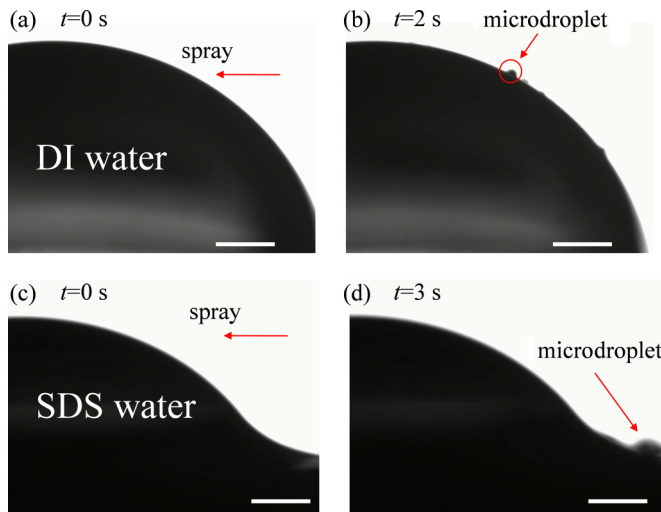


FIG. 11. Surface morphology of water droplet (a),(b) and SDS water droplet (c),(d) on lubricant-impregnated surface before spraying and after spraying. The scale bar in figure is 0.5 mm.

- [1] P. Kim, T. S. Wong, J. Alvarenga, M. J. Kreder, W. E. Adorno-Martinez, and J. Aizenberg, Liquid-infused nanostructured surfaces with extreme anti-ice and anti-frost performance, *ACS Nano* **6**, 6569 (2012).
- [2] Y. H. Jiang, C. Machado, S. Savarirayan, N. A. Patankar, and K. C. Park, Onset time of fog collection, *Soft Matter* **15**, 6779 (2019).
- [3] A. T. Paxson, J. L. Yague, K. K. Gleason, and K. K. Varanasi, Stable dropwise condensation for enhancing heat transfer via the initiated chemical vapor deposition (iCVD) of grafted polymer films, *Adv. Mater.* **26**, 418 (2014).
- [4] S. Sett, P. Sokalski, K. Boyina, L. N. Li, K. F. Rabbi, H. Auby, T. Foulkes, A. Mahvi, G. Barac, L. W. Bolton, and N. Miljkovic, Stable dropwise condensation of ethanol and hexane on rationally designed ultrascaleable nanostructured lubricant-infused surfaces, *Nano Lett.* **19**, 5287 (2019).
- [5] U. Lehmann, C. Vandevyver, V. K. Parashar, and M. A. M. Gijs, Droplet-based DNA purification in a magnetic lab-on-a-chip, *Angew. Chem. Int. Ed.* **45**, 3062 (2006).
- [6] L. L. Wang, L. P. Heng, and L. Jiang, Temperature-responsive anisotropic slippery surface for smart control of the droplet motion, *ACS Appl. Mater. Interfaces* **10**, 7442 (2018).
- [7] J. H. Wang, Y. Huang, K. You, X. Yang, Y. Song, H. Zhu, F. Xia, and L. Jiang, Temperature-driven precise control of biological droplet's adhesion on a slippery surface, *ACS Appl. Mater. Interfaces* **11**, 7591 (2019).
- [8] P. Che, L. Heng, and L. Jiang, Lubricant-infused anisotropic porous surface design of reduced graphene oxide toward electrically driven smart control of conductive droplets' motion, *Adv. Funct. Mater.* **27**, 1606199 (2017).
- [9] K. Ichimura, S. K. Oh, and M. Nakagawa, Light-driven motion of liquids on a photoresponsive surface, *Science* **288**, 1624 (2000).
- [10] P. Capobianchi, M. Lappa, and M. S. Oliveira, Deformation of a ferrofluid droplet in a simple shear flow under the effect of a constant magnetic field, *Comput. Fluids* **173**, 313 (2018).
- [11] M. R. Hassan, J. Zhang, and C. Wang, Deformation of a ferrofluid droplet in simple shear flows under uniform magnetic fields, *Phys. Fluids* **30**, 092002 (2018).
- [12] C. Rigoni, D. Ferraro, M. Carlassara, D. Filippi, S. Varagnolo, M. Pierno, D. Talbot, A. Abou-Hassan, and G. Mistura, Dynamics of ferrofluid drops on magnetically patterned surfaces, *Langmuir* **34**, 8917 (2018).
- [13] A. Li, H. Z. Li, Z. Li, Z. P. Zhao, K. X. Li, M. Z. Li, and Y. L. Song, Programmable droplet manipulation by a magnetic-actuated robot, *Sci. Adv.* **6**, eaay5808 (2020).
- [14] G. Huang, M. Li, Q. Yang, Y. Li, H. Liu, H. Yang, and F. Xu, Magnetically actuated droplet manipulation and its potential biomedical applications, *ACS Appl. Mater. Interfaces* **9**, 1155 (2017).
- [15] Z. Long, A. M. Shetty, M. J. Solomon, and R. G. Larson, Fundamentals of magnet-actuated droplet manipulation on an open hydrophobic surface, *Lab Chip* **9**, 1567 (2009).
- [16] L. Mats, R. Young, G. Gibson, and R. D. Oleschuk, Magnetic droplet actuation on natural (Colocasia leaf) and fluorinated silica nanoparticle superhydrophobic surfaces, *Sens. Actuators B* **220**, 5 (2015).
- [17] P. Agrawal, T. T. Salomons, D. S. Chiriac, A. C. Ross, and R. D. Oleschuk, Facile actuation of organic and aqueous droplets on slippery liquid-infused porous surfaces for the application of on-chip polymer synthesis and liquid-liquid extraction, *ACS Appl. Mater. Interfaces* **11**, 28327 (2019).
- [18] J. Doodoo and A. A. Stokes, Shaping and transporting diamagnetic sessile drops, *Biomicrofluidics* **13**, 064110 (2019).
- [19] K. Piroird, C. Clanet, and D. Quere, Magnetic control of leidenfrost drops, *Phys. Rev. E* **85**, 056311 (2012).
- [20] A. Tuteja, W. Choi, M. L. Ma, J. M. Mabry, S. A. Mazzella, G. C. Rutledge, G. H. McKinley, and R. E. Cohen, Designing superoleophobic surfaces, *Science* **318**, 1618 (2007).
- [21] Y. Lu, S. Sathasivam, J. Song, C. R. Crick, C. J. Carmalt, and I. P. Parkin, Robust self-cleaning surfaces that function when exposed to either air or oil, *Science* **347**, 1132 (2015).
- [22] T. S. Wong, S. H. Kang, S. K. Tang, E. J. Smythe, B. D. Hatton, A. Grinthal, and J. Aizenberg, Bioinspired self-repairing slippery surfaces with pressure-stable omniphobicity, *Nature (London)* **477**, 443 (2011).
- [23] A. Lafuma and D. Quéré, Slippery pre-suffused surfaces, *Europhys. Lett.* **96**, 56001 (2011).
- [24] J. D. Smith, R. Dhiman, S. Anand, E. Reza-Garduno, R. E. Cohen, G. H. McKinley, and K. K. Varanasi, Droplet mobility on lubricant-impregnated surfaces, *Soft Matter* **9**, 1772 (2013).

- [25] S. Hardt and G. McHale, Flow and drop transport along liquid-infused surfaces, *Annu. Rev. Fluid Mech.* **54**, 83 (2022).
- [26] N. Bjelobrk, H. L. Girard, S. B. Subramanyam, H. M. Kwon, D. Quere, and K. K. Varanasi, Thermocapillary motion on lubricant-impregnated surfaces, *Phys. Rev. Fluids* **1**, 063902 (2016).
- [27] J. L. Zhu, W. Y. Shi, T. S. Wang, and L. Feng, Spontaneous thermocapillary motion of condensation droplets, *Appl. Phys. Lett.* **116**, 243703 (2020).
- [28] See Supplemental Material at <http://link.aps.org/supplemental/10.1103/PhysRevFluids.7.053602> for movies showing motion of DI water droplet on SLIPS, confirmation of the noncloaking feature of SDS water droplet on SLIPS, and motion of SDS water droplet on a slippery surface infused with 10cSt silicone oil.
- [29] V. B. Varma, A. Ray, Z. M. Wang, Z. P. Wang, and R. V. Ramanujan, Droplet merging on a lab-on-a-chip platform by uniform magnetic fields, *Sci. Rep.* **6**, 37671 (2016).
- [30] Q. A. Pankhurst, J. Connolly, S. K. Jones, and J. Dobson, Applications of magnetic nanoparticles in biomedicine, *J. Phys. D* **36**, R167 (2003).
- [31] G. P. Zhu, N. T. Nguyen, R. V. Ramanujan, and X. Y. Huang, Nonlinear deformation of a ferrofluid droplet in a uniform magnetic field, *Langmuir* **27**, 14834 (2011).
- [32] P. K. Roy, E. Bormashenko, M. Frenkel, I. Legchenkova, and S. Shoval, Magnetic field induced motion of water droplets and bubbles on the lubricant coated surface, *Colloids Surf. A* **597**, 124773 (2020).
- [33] J. H. Guan, G. G. Wells, B. Xu, G. McHale, D. Wood, J. Martin, and S. Stuart-Cole, Evaporation of sessile droplets on slippery liquid-infused porous surfaces (slips), *Langmuir* **31**, 11781 (2015).
- [34] Y. X. Li, C. Diddens, T. Segers, H. Wijshoff, M. Versluis, and D. Lohse, Evaporating droplets on oil-wetted surfaces: suppression of the coffee-stain effect, *Proc. Natl. Acad. Sci. USA* **117**, 16756 (2020).
- [35] A. A. Günay, S. Sett, Q. Ge, T. Zhang, and N. Miljkovic, Cloaking dynamics on lubricant-infused surfaces, *Adv. Mater. Interfaces* **7**, 2000983 (2020).